Moisture sources and dynamics over southeastern Tibetan Plateau reflected in dual water vapor isotopes

Zhongyin Cai[1*], Rong Li[1], Cheng Wang[1], Qiukai Mao[1], Lide Tian[1]

[1]Institute of International Rivers and Eco-security, Yunnan Key Laboratory of International Rivers and Transboundary Eco-security, Ministry of Education Key Laboratory for Ecosecurity of Southwest China, Yunnan University, Kunming, China

*Corresponding author: Zhongyin Cai (czypil@gmail.com and z.cai@ynu.edu.cn)

Abstract

The southeastern Tibetan Plateau (SETP) has experienced a significant drying trend in recent decades, likely linked to changes in moisture sources. Water vapor isotopes are valuable tracers of the atmospheric water cycle, yet their interpretation is hindered by ambiguities in atmospheric controls. To investigate the role of ocean surface evaporation, continental air mass intrusion, and rain-vapor interaction, we present a three-year daily time series of near-surface vapor δ^{18}O and d-excess from the SETP station. Our analysis reveals that apparent negative correlations between d-excess and relative humidity over the Indian Ocean are primarily driven by similar seasonal patterns, which become insignificant or marginal when examined seasonally. This result underscores the need for caution in interpreting d-excess as a conservative tracer of ocean surface evaporation. Instead, we identify local and upstream specific humidity as the primary determinant of non-monsoon season d-excess variability, influenced by the

22   intrusion of cold and dry air from upper levels. During the summer monsoon season, both d-excess and $\delta^{18}O$ reflect

23   the effect of raindrop evaporation during transport, which decreases $\delta^{18}O$ but increases d-excess. These findings

24   provide new insights into the use of water isotopes to track moisture sources and dynamics over the SETP,

25   particularly under varying seasonal circulation systems. Particularly, the findings for d-excess will contribute to our

26   understanding of different moisture sources and provide a framework for interpreting d-excess in various

27   hydroclimatic applications, including ice core studies.

29   **1 Introduction**

30   The Tibetan Plateau (TP) and its surrounding regions, known as the Third Pole and the Asian Water Tower,

31   plays a crucial role in supplying water to major Asian rivers, including the Mekong, Salween, Ganges, Yarlung

32   Zangbo, among others, sustaining ecosystems and populations across the continent (Immerzeel et al., 2020; Yao et

33   al., 2022). In recent decades, the water balance on the TP has undergone significant changes ~~under the backdrop of~~

34   global warming (Yao et al., 2022). Notably, the southeastern TP (SETP) is experiencing a drying trend while wetting

35   in the north (Jiang et al., 2023; Zhang et al., 2023; Yao et al., 2022). Atmospheric water vapor is the primary input

36   to the hydrological system, making it essential to understand its sources and dynamics to diagnose regional water

37   imbalances. Using a Lagrangian vapor tracking method, Zhang et al. (2023) suggested that the drying trend is

38   associated with meteorological droughts propagating from moisture source regions. However, their conclusions and

39   methodology are subjects of ongoing debate (Zhang et al., 2025; ~~Zhao et al., 2025). Water stable isotopes are natural~~

40   ~~tracers of the water cycle, offering~~ valuable insights into moisture sources and dynamics (Bowen et al., 2019;

41   Galewsky et al., 2016). These isotopes have been intensively studied on the TP in precipitation, surface water, and

42   ice cores (Yao et al., 2013; Thompson et al., 2024; Bershaw, 2018). However, the interpretation of these isotopic

43 signals remains challenging due to complex fractionation processes and shifting circulation systems between

44 summer monsoon and westerlies.

45   Recent studies have confirmed that monsoon convection at upstream along moisture transport pathways, rather

46 than local precipitation amount, controls summer monsoon season precipitation $\delta^{18}O$ over southern TP (Cai et al.,

47 2017; He et al., 2015). This is related to the "amount effect" (Dansgaard, 1964), where higher precipitation leads to

48 lower $\delta^{18}O$ values due to continuous rainout associated with stronger convection, following the Rayleigh distillation

49 (Cai and Tian, 2016; Scholl et al., 2009; Vuille et al., 2003). Additionally, interactions between rain and water vapor

50 play a significant role in depleting the lower tropospheric vapor isotopes (Risi et al., 2008a; Kurita et al., 2011; Cai

51 et al., 2018; Lee and Fung, 2008). While the regional amount effect prevails during the monsoon season, this

52 relationship weakens or reverses in the non-monsoon season when it is dominated by westerlies. This variability

53 suggests additional controls such as moisture source variability, kinetic fractionation, or shifts in atmospheric

54 circulation patterns (Breitenbach et al., 2010; Cai and Tian, 2020; Guo et al., 2024; Yao et al., 2013).

55   Observations of vapor isotopes could help disentangle the different processes involved in the amount effect,

56 particularly through examining the secondary parameter deuterium excess (d-excess). The d-excess, defined by

57 Dansgaard (1964) as δ^2H - $8\delta^{18}O$, primarily reflects the effects of kinetic fractionation. During rainout process,

58 equilibrium fractionation is the dominant mechanism, whereas raindrop evaporation is associated with kinetic

59 fractionation. Further, limited precipitation during non-monsoon seasons makes it challenging to study a full

60 seasonal cycle of the atmospheric water cycle, which can be compensated by continuous monitoring of vapor

61 isotopes. While a few stations on the TP have monitored isotopic compositions in the vapor phase (Tian et al., 2020;

62 Dai et al., 2021; Chen et al., 2024; Yu et al., 2016; Yu et al., 2015), there is limited knowledge about vapor d-excess.

63   Both theoretical predictions and observations over ocean surfaces indicate that d-excess reflects ocean surface

64 evaporation conditions such as sea surface temperature (SST) and relative humidity normalized to SST (RH$_{SST}$)

65 (Merlivat and Jouzel, 1979; Bonne et al., 2019; Liu et al., 2014; Craig and Gordon, 1965). These relationships are

66 frequently invoked in interpreting d-excess over the TP (Zhao et al., 2012; Shao et al., 2021; Chen et al., 2024; Liu

67 et al., 2024). For instance, Shao et al. (2021) showed significant correlations between an ice core d-excess record

68 from the central TP and RH_{SST} over the northern Bay of Bengal (BOB) and Arabian Sea (AS). However, the

69 correlation coefficient was only -0.44 with a steep slope of -0.99‰ %$^{-1}$. This contrasts with oceanic regions where

70 the slope typically ranges from -0.3‰ %$^{-1}$ to -0.6‰ %$^{-1}$ (Bonne et al., 2019; Liu et al., 2014; Benetti et al., 2014;

71 Uemura et al., 2008), suggesting additional complexities over terrestrial areas. Moreover, many studies have

72 suggested that d-excess at terrestrial sites is not a conservative tracer of evaporation conditions from oceanic source

73 regions (Fiorella et al., 2018; Aemisegger et al., 2014; Welp et al., 2012; Wei and Lee, 2019; Samuels‐Crow et al.,

74 2014). In addition, ice core d-excess values at high altitudes are generally higher than those observed in precipitation

75 at lower altitudes on the TP (Shao et al., 2021; Tian et al., 2001; Zhao et al., 2012; Joswiak et al., 2013; Zhao et al.,

76 2017; Thompson et al., 2000). The reason for this discrepancy remains unclear, highlighting the need for further

77 research to understand the mechanism driving these differences.

78 Mountain valleys in the SETP are considered significant pathways for transporting water vapor into the TP

79 (Araguás-Araguás et al., 1998; Tian et al., 2007; Yao et al., 2013). To investigate these processes, we initiated a

80 water vapor sampling campaign at the South-East Tibetan Plateau Station for integrated observation and research

81 of alpine environment (SETP station) in June 2015. We aim to study the moisture sources and dynamics and their

82 influence on vapor isotope compositions across different seasons. To achieve these goals, we explored the

83 relationships between vapor isotopes and oceanic evaporation conditions, continental air mass intrusions, as well as

84 rain-vapor interactions during different seasons. Finally, we discuss the implications of our findings for interpreting

85 ice core records.

86   **2 Data and methods**

87   **2.1 Atmospheric water vapor sampling**

88   Vapor samples were collected at the SETP station (29°46'N, 94°44'E, 3326 m above sea level, and Fig. S1)

89   using a cryogenic trapping method. The sampling system includes an air pump, a linked-ball-shaped glass cold trap,

90   and an electric-powered system that creates and maintains a cold environment filled by 95% ethanol as cold as

91   below -80 °C. Ambient air was pumped from an inlet positioned about 8 m above ground level through a Teflon

92   tube to a glass trap maintained at an operational temperature of -70 °C. The airflow rate was set to ~5 L/min,

93   allowing the collection of 10-20 ml of water samples during each sampling session. Sampling durations were

94   adjusted seasonally: 24 hours in summer and extended to 48 hours in winter when necessary to ensure adequate

95   sample volume. Samples were collected at 20:00 Beijing Standard Time (12:00 UTC). The efficiency of the trapping

96   method was verified by connecting an additional cold trap to the system, which showed no visible condensation in

97   the additional cold trap (Yu et al., 2015). Further validation was achieved through comparisons with direct

98   measurements using a Picarro L2130-i Cavity Ring Down Spectroscopy (CRDS) at Lhasa, southern TP, confirming

99   the reliability of this method for atmospheric water vapor sampling (Tian et al., 2020).

100   The sampling campaign ran from 25 June 2015 to 14 June 2018, yielding a total of 742 samples. These samples

101   were stored frozen until analysis. Samples collected before 28 June 2016 were measured at the Key Laboratory of

102   Tibetan Plateau Earth System, Environment and Resources, Institute of Tibetan Plateau Research, Chinese Academy

103   of Sciences by a Picarro L2130-i analyzer. Samples collected after 28 June 2016 were measured at the Institute of

104   International River and Eco-security, Yunnan University by a Picarro L2140-i analyzer. The isotopic values were

105   calibrated using three standard waters, with detailed calibration procedures described by Liu et al. (2024). The

106   measurements are expressed relative to Vienna Standard Mean Ocean Water 2 (VSMOW2), with precisions of 0.1‰

107   for $\delta^{18}O$, 0.4‰ for δ^2H, and 1.2‰ for d-excess.

2.2 Meteorological data

Daily local meteorological data prior to 2018, including precipitation amount, air temperature, air pressure, and relative humidity at the SETP station, were obtained from the National Tibetan Plateau/Third Pole Environment Data Center (Luo, 2018). Specific humidity (q) at the SETP station was calculated using air temperature, air pressure, and relative humidity data following established equations outlined in (Huang, 2018). Consistent with Yao et al. (2013), we defined June-September (JJAS) as the summer monsoon season. In contrast, November-April (Nov-Apr) was designated as the non-monsoon season, with May and October considered transition periods between the two seasons.

We further obtained meteorological variables such as 2-meter air temperature, 2-meter dew point temperature, SST, and others at 0.25°×0.25° and hourly resolution from the European Centre for Medium-Range Weather Forecasts fifth generation reanalysis (ERA5) (Hersbach et al., 2019). RH_{SST} is estimated using ERA5 data: $RH_{SST} = e_{air}/e_{sat}$, where e_{air} is vapor pressure of air and e_{sat} is saturation vapor pressure with respect to SST. Additionally, precipitation data at 0.1°×0.1° and half-hourly resolution were obtained from the Integrated Multi-satellitE Retrievals for GPM (V07) dataset (Huffman et al., 2023). Moreover, meteorological data at 1°×1° and 3-hourly resolution from the Global Data Assimilation System (GDAS) were used to calculate backward trajectories (see Section 2.4 for details).

Statistical analyses primarily involved linear correlations and regressions, with the coefficient of determination (R^2) used to quantify the variance explained by each variable. In addition, we also used composite analysis to reveal relationships between variables. For example, to identify general patterns in backward trajectories associated with d-excess exceeding 30‰, all the days with such high d-excess were compiled into a collection. A composite map of trajectories from this collection was then constructed to reveal typical pathways under these conditions.

2.3 Theoretical framework for the understanding of isotope compositions and humidity

Besides complex atmospheric circulation models, the evolution of vapor isotope compositions during different moistening and dehydration processes can be predicted through a compilation of atmospheric processes such as condensation, mixing, and raindrop evaporation (Noone, 2012; Worden et al., 2007; Galewsky et al., 2016). These process shape distinct pathways of isotopic evolution in relation to atmospheric humidity.

The Rayleigh distillation model describes the progressive condensation of water vapor (Dansgaard, 1964). The isotope composition of remaining vapor, denoted as δ, can be expressed as $\delta = (1 + \delta_0)(q/q_0)^{\alpha-1} - 1$, where q is the specific humidity, and α is the fractionation factor. A subscript of 0 refers to the initial condition of the air mass. Raindrop evaporation introduces further complexity. As raindrops form at higher altitudes where vapor is depleted in heavy isotopes, their partial evaporation affects the surrounding vapor, leading to isotope values lower than those predicted by Rayleigh models (Risi et al., 2008a; Worden et al., 2007). This effect gives rise to "super-Rayleigh" trajectories, characterized by an inflated effective fractionation factor (α_e), defined as $\alpha_e = (1 + \phi)\alpha$, where ϕ quantifies deviations from equilibrium. Notably, Worden et al. (2007) and Noone (2012) have given different equations for such deviations, and this study aligns with the formulations by Noone (2012).

Air mass mixing also influences humidity and isotopic compositions ~~through mass balance principles~~. When a dry air mass mixes with a moist one, the specific humidity of the mixed air can be described as $q = f_{dry}q_{dry} + f_{moist}q_{moist}$, where f represents the fraction of each air mass, with $f_{dry} + f_{moist} = 1$. Isotopic compositions are similarly derived by solving mass balance equations for the light and heavy isotopes, resulting in a hyperbolic relationship between δ and q. In other words, $\delta \times q$ and q should have a linear relationship in the mixing process (Fiorella et al., 2018). The intercept of the regression between δ and $1/q$ or the slope between $\delta \times q$ and q provides an estimate of the moist end member's isotope composition (Keeling, 1958).

Assuming a surface temperature of 25 °C and relative humidity of 85%, we utilize the evaporation model by

151 Craig and Gordon (1965) to determine the isotopic composition of ocean evaporation. This results in $\delta^{18}O$ = -11.5‰,

152 δ^2H = -81.4‰, and d-excess = 10.6‰. These values serve as the wet end member for modeling moistening process

153 through mixing with ocean evaporation. For the dry end member, we consider a dehydrated air mass from the

154 Rayleigh curve at q = 0.5 g/kg, $\delta^{18}O$ = -60.3‰, and δ^2H = -418.0‰ (Fig. S2). The dehydration process via

155 condensation is initiated at a relative humidity of 80% on the mixing line. Similarly, "super-Rayleigh" distillation

156 involving partial rain evaporation also begins from this starting point. We explore two "super-Rayleigh" scenarios:

157 Rain_evap_A assumes 2% rain evaporation, while Rain_evap_B assumes 5%, based on equations from Noone

158 (2012). Additionally, we consider the influence of evapotranspiration over south Asia and the TP on atmospheric

159 humidity and vapor isotope compositions over SETP. Quantifying isotopic compositions of land surface

160 evapotranspiration is challenging. Given precipitation $\delta^{18}O$ over south Asia generally ranges from -1.0‰ to -5.0‰

161 (Bowen and Wilkinson, 2002; Terzer-Wassmuth et al., 2021) and transpiration constitutes two-thirds or more of

162 evapotranspiration (Cao et al., 2022; Han et al., 2022; Good et al., 2015), we assume a $\delta^{18}O$ value of -5.0‰ as an

163 upper bound for land surface evapotranspiration. Similarly, we assume a d-excess of 15.0‰ for this wet end member.

164 **2.4 Backward trajectory and moisture source diagnostic**

165 To investigate air mass transport and diagnose moisture sources and pathways toward SETP, we calculated

166 backward trajectories using the Hybrid Single-Particle Lagrangian Integrated Trajectory model (HYSPLIT) (Stein

167 et al., 2015). Trajectory calculations were driven by meteorological data from the GDAS. Air parcels were released

168 from 5 locations: the study site and points displaced 0.2° in each cardinal direction. These releases occurred at 7

169 different vertical levels: 10, 50, 100, 200, 300, 400, and 500 m above ground level. For each day during the sampling

170 campaign, trajectories were initiated every 3 hours to calculate 10-day backward trajectories, resulting in 280

171 trajectories per day. Geographical and meteorological variables, including location, pressure, temperature, specific

172 humidity, rainfall amount, boundary layer height, and terrain height along the trajectories, were stored at hourly

173   intervals.

174   To quantify moisture contributions along trajectories to SETP's humidity, we applied the Lagrangian moisture

175   source diagnostic method developed by Sodemann et al. (2008). This method uses mass balance principles along

176   trajectories, interpreting increases in specific humidity (forward in time) as moisture uptake and decreases as

177   moisture loss due to precipitation. It also accounts for the reduced contribution of earlier moisture uptake due to

178   precipitation en route. We previously adapted this method to identify moisture sources for precipitation in sub-

179   regions of South Asia and East Asia (Cai et al., 2018; Cai and Tian, 2020).

180   The diagnostic results indicated that approximately 5% of the moisture arriving at SETP remained unattributed,

181   confirming that 10-day trajectories are sufficient to diagnose most moisture sources. Unlike previous applications

182   focused on identifying evaporative moisture sources from the Earth's surface, this study emphasizes the contribution

183   of air parcels themselves to SETP's humidity. This variable is readily available from the diagnostic method, where

184   changes in air parcel contributions within the boundary layer between time steps represent moisture uptake from

185   the surface.

186   The moisture contribution of an air parcel to SETP's humidity is a measure of the importance of upstream air.

187   We calculated weighted-mean values for key variables by using the moisture contribution of the air parcel along

188   trajectories as the weight. We also applied K-means clustering to group trajectories, helping to identify major

189   transport pathways. When calculating the mean trajectory for each cluster and meteorological variables along each

190   mean trajectory, the moisture contribution of the air parcel is also considered as the weight to calculate weighted-

191   means.

3 Results

3.1 General characteristics of vapor δ^{18}O, d-excess, and local meteorological variables

In general, δ^{18}O values are at lower levels during the summer monsoon season and higher levels during the non-monsoon season (Fig. 1a). Mean δ^{18}O values are -18.4‰ for the non-monsoon season, -23.3‰ for the summer monsoon season, -16.9‰ for May, and -22.8‰ for October. δ^{18}O shows a dramatic decrease at the onset of the summer monsoon. Conversely, from the end of the summer monsoon season to spring and early summer, δ^{18}O shows a gradual increase trend. Although the amount effect significantly influences this region, the seasonal variation of δ^{18}O does not strictly align with local precipitation patterns. For instance, while local precipitation ceases clearly after the summer monsoon (Fig. 1e), δ^{18}O remains at relatively low levels. This behavior is consistent with precipitation δ^{18}O in SETP, northeast India, and Bangladesh (Yao et al., 2013; Cai and Tian, 2020; Yang et al., 2017).

In contrast to δ^{18}O, d-excess displays different seasonal dynamics. The d-excess values are lower during the summer monsoon season and higher during non-monsoon periods (Fig. 1b). Mean d-excess values are 18.3‰ for the non-monsoon season, 11.9‰ for the summer monsoon season, 13.7‰ for May, and 14.9‰ for October. However, the timing of seasonal transitions in d-excess differs from that of δ^{18}O. The highest d-excess values generally occur during winter months when air temperature and relative humidity (RH) are at their lowest levels (Fig. 1c and 1d). Furthermore, d-excess starts to decrease in spring, earlier than the sharp drop in δ^{18}O at the onset of the summer monsoon.
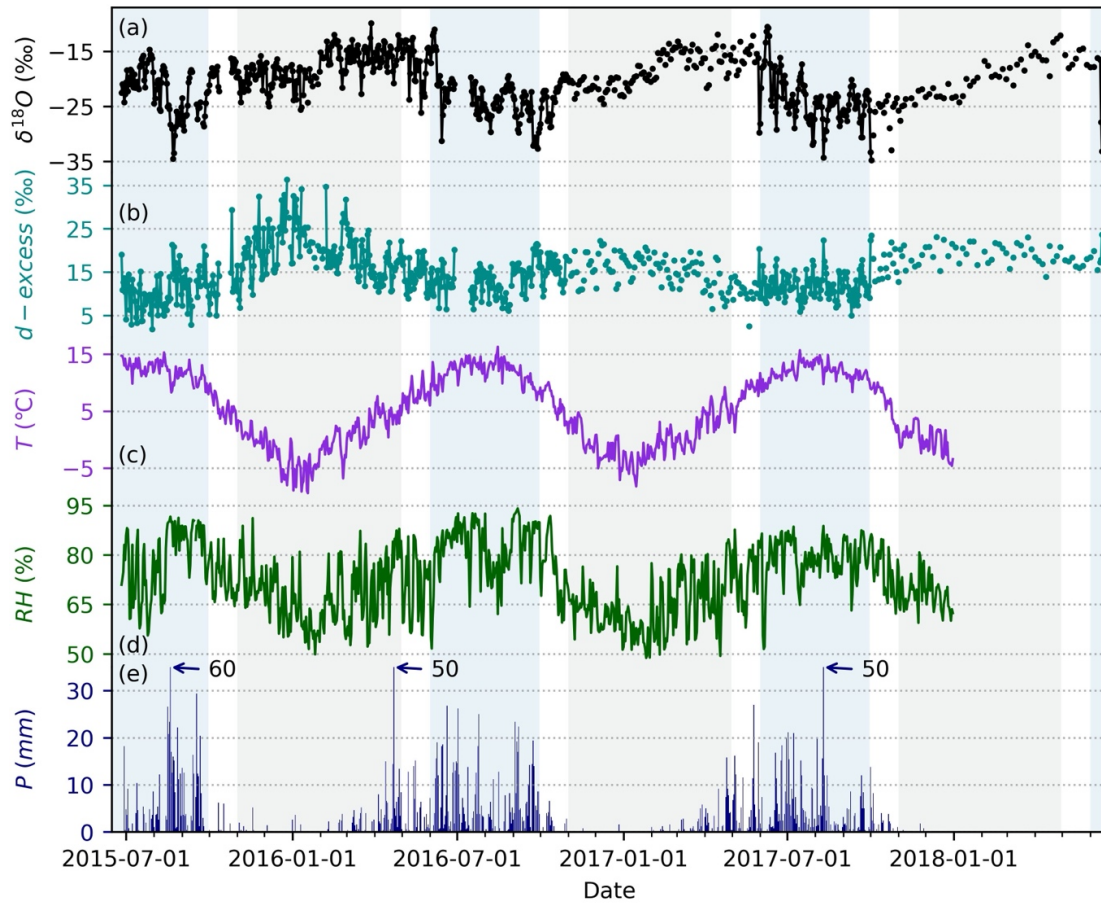
Figure 1. Time series of ~~observed~~ vapor δ¹⁸O, *d*-excess, and daily local meteorological variables from 2015-2018: (a) δ¹⁸O, (b) *d*-excess, (c) air temperature, (d) relative humidity (RH), and (e) precipitation amount. Light blue shading highlights the summer monsoon season, while light steel blue shading highlights the non-monsoon season.

The linear relationship between paired $\delta^{18}O$ and δ^2H values, along with their position relative to the global meteoric water line (GMWL, $\delta^2H = 8\delta^{18}O + 10$) (Craig, 1961), provides additional insights into isotopic fractionation processes (Putman et al., 2019). The local vapor line (LVL), estimated from all δ^2H and $\delta^{18}O$ data points, is $\delta^2H = 7.96\delta^{18}O + 14.04$ ($R^2 = 0.98$). This LVL plots above but approximately parallel with the GMWL. This relatively higher intercept of LVL reflects the continental location of the site and additional kinetic fractionation after ocean evaporation. The δ^2H-$\delta^{18}O$ relationship also varied seasonally. During the non-monsoon season, the LVL

221 is $\delta^2H = 7.58\delta^{18}O + 10.61$ ($R^2 = 0.96$), while during the summer monsoon season, it shifts to $\delta^2H = 7.53\delta^{18}O + 0.91$

222 ($R^2 = 0.99$). Non-monsoon data primarily plot above both the GMWL and the overall LVL. Conversely, most

223 monsoon season isotope data fall below the overall LVL, though the lowest δ-value points during this period are

224 positioned above the overall LVL, suggesting additional kinetic fractionation such as rain evaporation (He et al.,

225 2024). Vapor isotopes for May resemble those of the non-monsoon season but align more closely with both the

226 GMWL and LVL, whereas data for October exhibit behaviors similar to the monsoon season observations.

227
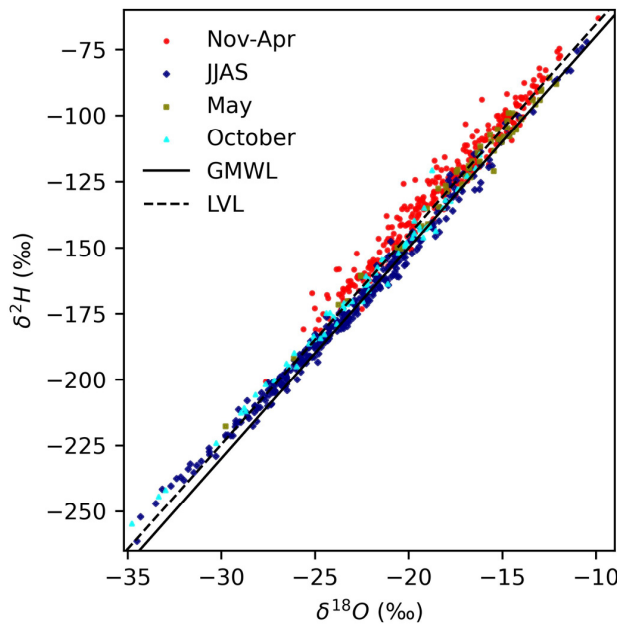
Figure 2. Relationship between vapor δ²H and δ¹⁸O. The data is presented for different seasons: non-monsoon (Nov-Apr) as red dots, summer monsoon (JJAS) as navy diamonds, May as olive squares, and October cyan trangles. The solid line indicates the global meteoric water line (GMWL). The dashed line indicates the local vapor line (LVL) estimated from all δ²H and δ¹⁸O data points.

232 The relationships between $\delta^{18}O$ and specific humidity (q) further indicate distinct seasonal patterns in moisture

233 dynamics (Fig. 3a). Due to unavilability of local meteorological data for 2018, our analyses focused on data

234 collected before this year.. During the non-monsoon season, particularly in winter months, most data points are

235 positioned above the Rayleigh distillation line but below a mixing line that represents an upper bound of

236   hypothetical evapotranspiration over South Asia. This suggests a mix between a dry end member and a moist end

237   member. In contrast, during the summer monsoon season, data predominately fall below the Rayleigh line,

238   influenced by "super-Rayleigh" processes linked to rain evaporation.

239   Futher insights come from examing $\delta \times q$ versus q relationships, which highlight seasonal contrasts in

240   moisture source signatures (Fig. S3). For the non-monsoon season, a simple estimation through the linear regression

241   between $\delta \times q$ and q suggests a moist end member with an $\delta^{18}O$ of -13.9‰ ± 0.6‰. The amount weighted annual

242   mean precipitation $\delta^{18}O$ at our site was about -14.5‰ (Yao et al., 2013). However, during the monsoon season, the

243   overall estimation of $\delta^{18}O$ for the moist end member through the linear regression between $\delta \times q$ and q is

244   significantly lower at -30.9‰ ± 1.8‰, pointing to an additional moisture source from rain evaporation that is more

245   depleted in heavy isotopes. These results align with the distribution of $\delta^{18}O$-q data below the Rayleigh line during

246   the summer monsoon season (Fig. 3a), underscoring the influence of different moisture sources and processes across

247   seasons.

248   The relationships between *d*-excess and *q* also reflect seasonal contrasts in moisture dynamics (Fig. 3b). During

249   non-monsoon season months, a negative correlation is observed where lower *q* corresponds to higher *d*-excess

250   values (Figs. 1 and 3b). This relationship is particularly pronounced under dry and cold conditions. In contrast,

251   during the summer monsoon season, no clear relationship between *d*-excess and *q* is apparent, with *d*-excess

252   showing considerable variability of approximately 20‰ at any given *q*. These findings suggest that *d*-excess is less

253   predictable using *q* compared to $\delta^{18}O$, except under low humidity levels.
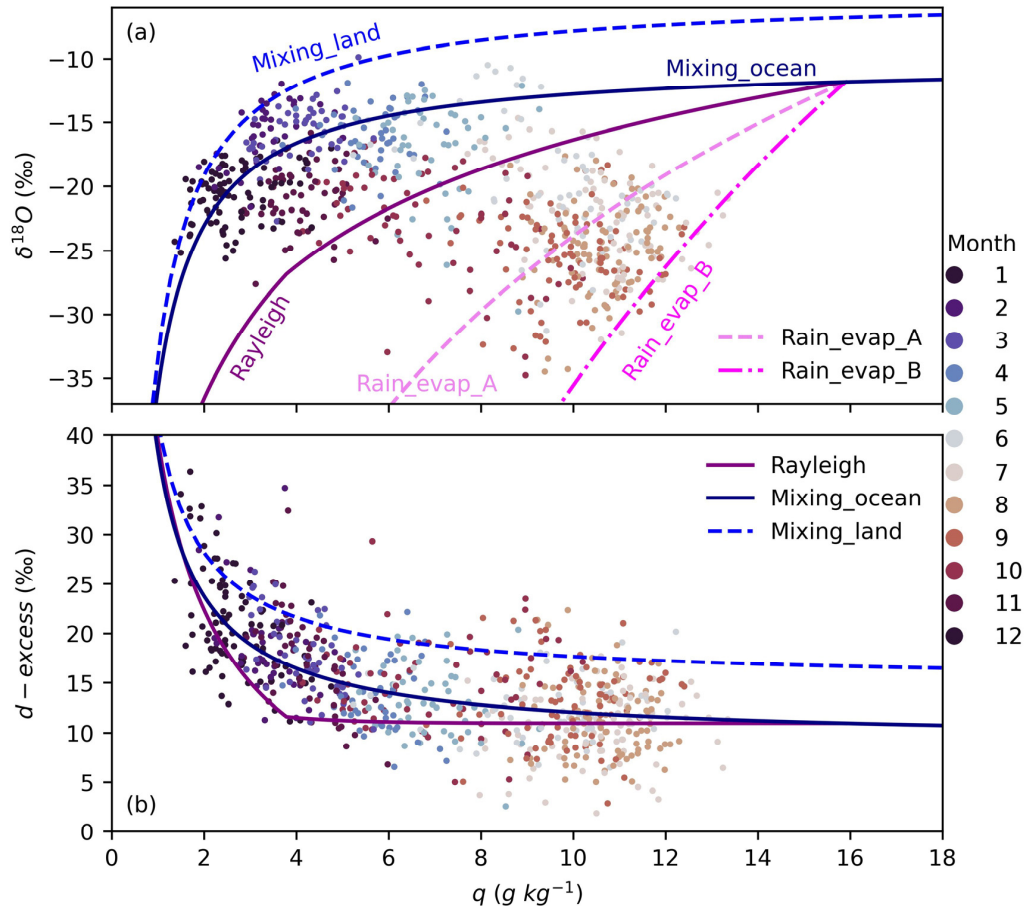
Figure 3. Relationships between vapor isotopes ($\delta^{18}O$ and *d*-excess) and specific humidity (*q*) from 2015-2017. (a) scatter plot of $\delta^{18}O$ against *q*. (b) scatter plot of *d*-excess against *q*. Each data point is color-coded by month. Reference lines correspond to those in Fig. S2; their interpretations is detailed in Fig. S2 and Section 2.3. Note that only data before 2018 are shown (see text for details).

3.2 Seasonal variability in moisture sources and transport pathways

To understand the drivers behind the seasonal variations in moisture dynamics, we analyzed the moisture sources and transport pathways during different seasons (Fig. 4). Our focus was on the contribution of moisture from historical air masses (last 10 days) to humidity at SETP.

During the non-monsoon season, moisture is mainly transported via two pathways: one originating from the west of SETP, carried by the westerlies (clusters Nov-Apr2 and Nov-Apr3), and another from the south, such as the

265   BOB (cluster Nov-Apr1). Quantitatively, the contributions frm these pathways are comparable, with 52.4% from

266   the southern pathway and 47.7% from the western branches combined. Interestingly, when considering only

267   trajectories without accounting for moisture contributions, all three clusters appear to originate from the west of

268   SETP (Fig. S4). This discrepancy highlights the importance of distinguishing between pure air mass transport and

269   actual moisture sources when interpreting trajectory data.

270   In contrast, during the summer monsoon season, moisture transport is predominantly from the south of SETP,

271   driven by the summer monsoon. The pathways observed in May share similarities with those of the non-monsoon

272   season, but with notable differences. Specifically, the second pathway during May (cluster May2) shifts southward

273   toward the AS compared to its counterpart during the non-monsoon (cluster Nov-Apr2). Similarly, while October's

274   air mass transport direction mirrors that of the non-monsoon, the moisture sources and pathways show greater

275   alignment with those of the summer monsoon season, albeit with a slight eastward shift (Figs. 4d and S4d).

276   Another notable aspect of the moisture source distributions is the dominant contribution from proximal

277   terrestrial regions, particularly those to the south of SETP (Fig. 4). For example, the 1% contour representing

278   moisture contributions from air parcels over each 1°×1° grid box does not extend into oceanic regions during any

279   of the four seasons. This indicates that surface evaporation from oceanic regions such as the BOB and AS contributes

280   minimally. Instead, most of the moisture originating over these oceanic regions is lost through precipitation before

281   reaching SETP, and what remains is replenished by evapotranspiration during transport over land. This finding raises

282   an important question: do the vapor isotopes measured at SETP still reflect the meteorological conditions at their

283   oceanic sources?
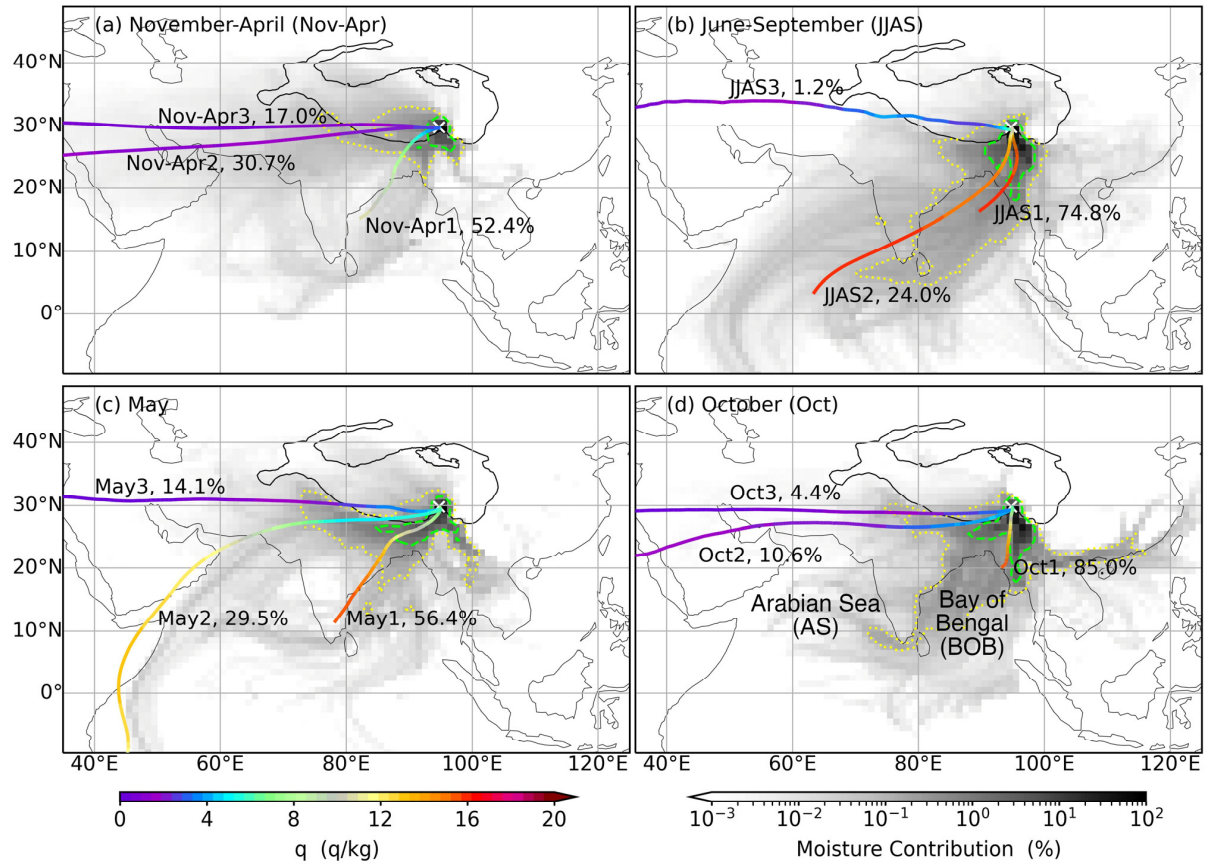
Figure 4. Moisture sources and transport pathways during different seasons from 2015-2017. (a) spatial distribution of relative contributions of moisture from all air parcels over each 1°×1° box (shading) to humidity at the SETP station, along with specific humidity (*q*) along mean trajectories (weighted by moisture contributions) for the non-monsoon season of November-April (Nov-Apr). (b-d) are the same as (a), but for the monsoon season of June-September (JJAS, b), May (c), and October (d), respectivley. The dotted yellow and dashed green contours indicate the moisture contribution at 0.1% and 1%, respectively. The yellow crosses indicate the location of the SETP station. The black solid lines denote the Tibetan Plateau with altitude contour at 3000 m.

3.3 Role of ocean surface evaporation conditions at seasonal and intraseasonal time scales

Relationships between *d*-excess and ocean surface evaporation conditions, such as RH_{SST} and SST, were

295 examined using data from 2015-2017 (Fig. 5a and Fig. S5a). Results indeed show negative correlations between d-

296 excess and RH_{SST} over northern Indian Ocean, particularly in the northern parts of AS and BOB (Fig. 5a).

297 Specifically, the regression slopes for this relationship across the northern Indian Ocean vary from higher than -

298 0.1‰ %$^{-1}$ to values below -0.6‰ %$^{-1}$.

299   Focusing on specific regions, the northern BOB (10-22°N and 80-99°E) and the eastern AS (7-20°N and 65-

300 78°E; Fig. 5a) exhibited regression slopes within the range (from -0.3‰ %$^{-1}$ to -0.6‰ %$^{-1}$) previously reported

301 (Uemura et al., 2008; Benetti et al., 2014; Liu et al., 2014; Bonne et al., 2019). For instance, the regional average

302 RH_{SST} in the eastern AS shows an overall regression slope of -0.49‰ %$^{-1}$ (r = -0.52 and p < 0.01) (Fig. 6a), while

303 the northern BOB has a slope of -0.52‰ %$^{-1}$ (r = -0.55 and p < 0.01) (Fig. 6b). However, upon closer inspection of

304 the d-excess- RH_{SST} plots (Fig. 6), it becomes evident that data points clustered according to different seasons,

305 implying that the apparent negative correlations might primarily stem from opposing seasonal trends. Similarly,

306 apparent negative correlations between d-excess and SST also emerge over the northern Indian Ocean (Fig. S5a).

307 Yet, both theoretical prediction (Merlivat and Jouzel, 1979) and in-situ observations above the ocean surface (Bonne

308 et al., 2019; Liu et al., 2014) suggest a positive correlation between d-excess and SST. These discrepancies lead us

309 to speculate that the overall correlations between SETP vapor d-excess and surface evaporation conditions over the

310 northern Indian Ocean are likely driven by seasonal variability.

311   The relationship between d-excess and RH_{SST} was further analyzed by distinguishing between the summer

312 monsoon and non-monsoon seasons. During the summer monsoon season, the negative correlation diminishes

313 significantly, with correlation coefficients dropping below 0.3 (Fig. 5b). In contrast, significant correlations present

314 during the non-monsoon season (Fig. 5c), potentially due to intraseasonal variations where d-excess peaks in winter

315 and decreases at the beginning and ending of the non-monsoon season (Fig. 1b), possibly accompanied by opposing

316 RH_{SST} trends. However, even during the non-monsoon season, the explained variance in d-excess remains low, at a

317 maximum of 10%-16% over the northern BOB. Similarly, correlations with SST over the northern Indian Ocean

318 also become negligible when seasons are considered separately (Fig. S5). In summary, vapor d-excess at SETP is

319 less likely a conservative tracer of surface evaporation conditions (neither RH$_{SST}$ nor SST) over the northern Indian

320 Ocean. Therefore, interpreting d-excess in meteoric water or paleo archives from the TP as a proxy for Indian Ocean

321 evaporation conditions should be approached with caution.

322
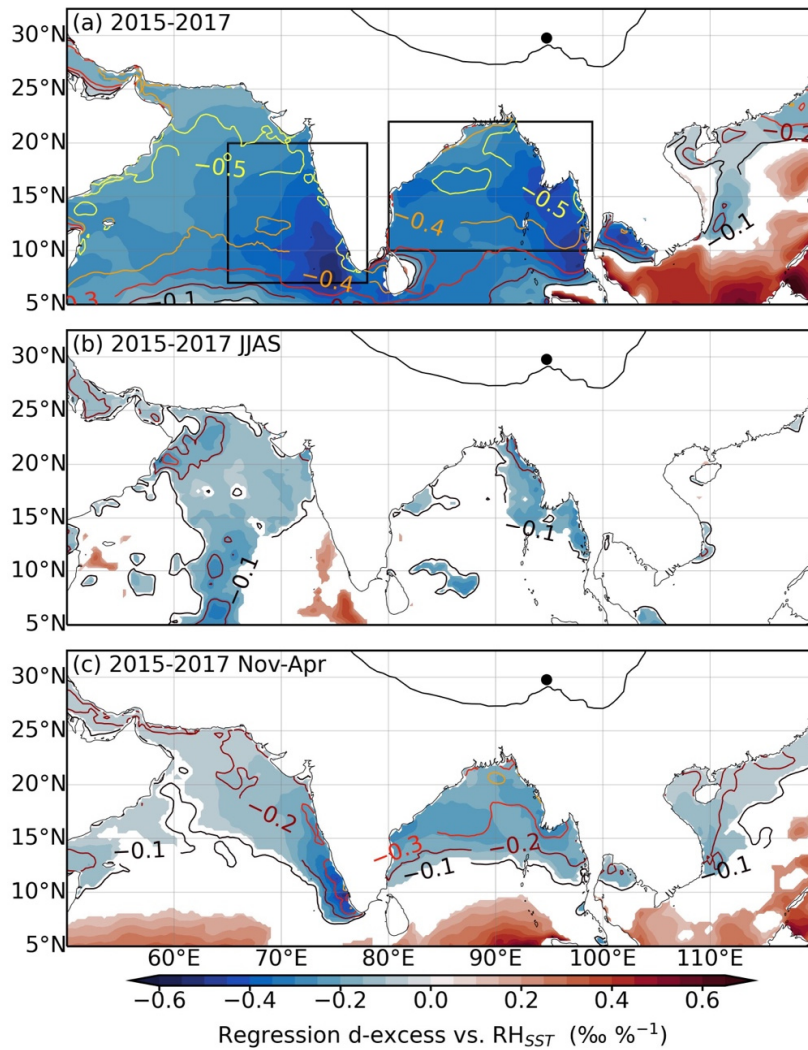
323 **Figure 5. Relationships between vapor d-excess and relative humidity scaled to sea surface temperature**

324 **(RH$_{SST}$). (a) regression of d-excess against RH$_{SST}$ (shading and only values significant at the 95% significance**

325 **level are shown) and correlation coefficients between them (contours at an interval of 0.1 and only negative**

 correlations are shown) for all the data from 2015-2017. (b) and (c) are the same as (a) but only for the data

327 within the summer monsoon season (JJAS) or the non-monsoon season (Nov-Apr), respectively. The black

328 dots indicate the location of the SETP station. The black solid lines denote the Tibetan Plateau with altitude

329 contour at 3000 m.

330
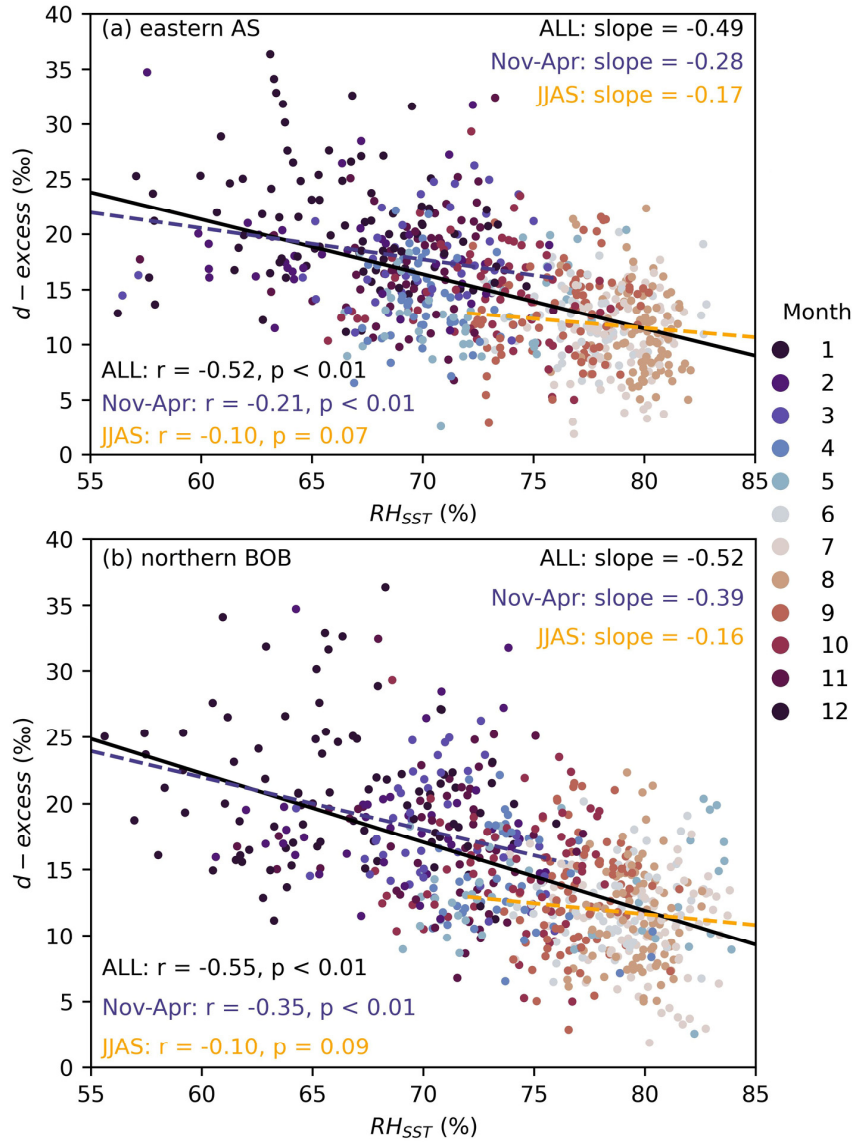
331 Figure 6. Relationships between SETP vapor *d*-excess and relative humidity normalized to sea surface

332 temperature (RH_{SST}) averaged over (a) eastern Arabian Sea (7-20°N and 65-78°E) and (b) Bay of Bengal (10-

333 22°N and 80-99°E) from 2015-2017. Each data point is color-coded by month. Solid black lines indicate the

334 **linear regression between all data points. Dashed orange lines indicate linear regression for data during the**

335 **non-monsoon season (Nov-Apr) and dashed dark blue lines for data during the summer monsoon (JJAS).**

336 **The slope (‰ %$^{-1}$), r, and p values for the three data groups are also shown.**

337 **3.4 Role of dry and cold air intrusion during the non-monsoon season**

338   Both theoretical predictions from the Rayleigh model and observations during the non-monsoon season suggest

339 that d-excess increases as q decreases when q reaches extremely low values (Fig. 2). In addition, results for both air

340 mass transport and moisture transport show the dominant role of the westerlies (Figs. S4a and 4a). Based on these

341 evidences, we propose that during the non-monsoon season, vapor isotopes are influenced by the mixing of cold

342 and dry air transported by westerlies from higher altitudes with surface vapor. Furthermore, surface vapor influenced

343 by recycled moisture from terrestrial evapotranspiration would further elevate d-excess at a given q (Fig. 3b).

344   We performed a composite analysis on moisture sources and transport pathways for the highest (higher than

345 30‰, and n = 10) and lowest (lower than 10‰, and n = 8) d-excess observations during the non-monsoon season

346 (Fig. 7). High d-excess values are primarily associated with moisture transported by westerlies from regions west

347 of SETP, such as over the TP and northwestern India. In addition, backward trajectories for these cases show air

348 masses characterized by extremely low q, reaching below 2 g kg^{-1} along the mean trajectories (weighted by moisture

349 contribution) over the TP (Fig. 7a). Conversely, for low d-excess cases, a significant portion of moisture transport

350 pathways shifts toward more humid regions, including northeast India, Bangladesh, and the BOB, with the L1

351 cluster accounting for 39.2% (Fig. 7b). This contrasting moisture transport pattern between high and low d-excess

352 cases aligns with our hypothesis that high d-excess is associated with dry and cold air transported by westerlies.
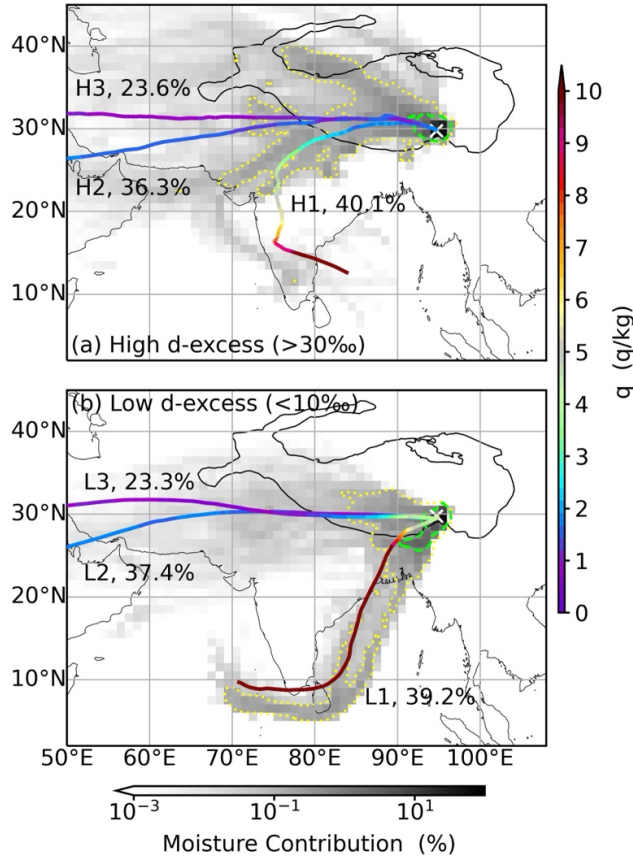
Figure 7. Composite of moisture sources and transport pathways for high and low _d_-excess days during the non-monsoon season of November-April. (a) spatial distribution of relative contribution of moisture from all air parcels over each 1°×1° box (shading) to humidity at the SETP station, along with specific humidity (_q_) along mean trajectories (weighted by moisture contributions) for _d_-excess values higher than 30‰ during the non-monsoon season (n = 10). (b) is the same as (a) but for _d_-excess lower than 10‰ (n = 8). ~~The~~ yellow crosses indicate the location of the SETP station. ~~The~~ black solid lines denote the Tibetan Plateau with altitude contour at 3000 m.

The influence of cold and dry air intrusions was further investigated through an analysis of relationships involving _d_-excess, local _q_, weighted-mean upstream _q_, weighted-mean upstream air temperature, and weighted-mean upstream air altitude (Fig. 8). Upstream variables represent weighted averages along the 10-day backward trajectory, where weights correspond to the moisture contribution at each time step (Section 2.4). The non-monsoon

365   season d-excess shows robust negative correlations with both local q (r = -0.65, p < 0.01) and upstream q (r = -0.67,

366   p < 0.01). Furthermore, low q is associated with air masses characterized by low temperatures and high altitudes

367   (Figs. 8c and 8d), which could also impact $\delta^{18}O$. Indeed, $\delta^{18}O$ during high d-excess cases is lower than during low

368   d-excess cases (at a significance level of 95.3%). The overall correlation coefficient between $\delta^{18}O$ and d-excess

369   during the non-monsoon season is -0.29 (p < 0.01). Notably, correlations between $\delta^{18}O$ and q are weaker compared

370   to those observed for d-excess, with local q showing r = 0.42 (p < 0.01) and upstream q showing r = 0.38 (p < 0.01).

371   The relationship between non-monsoon season $\delta^{18}O$ and humidity is mainly expressed as the relationship between

372     $\delta \times q$ and q (r = 0.82 for local q and r = 0.90 for upstream q). Spatial correlations between vapor isotopes ($\delta^{18}O$

373   and d-excess) and 2-meter air temperature as well as humidity measured by 2-meter dew point temperature also

374   support these findings (Fig. S6). Significant negative correlations between d-excess and dew point temperature exist

375   over southeastern TP, northeast India, and northern Bangladesh. In contrast, $\delta^{18}O$ shows significant positive

376   correlations with air temperature over the India subcontinent and northwestern Southeast Asia.

377   As shown in Fig. 3b, extremely high d-excess values are predicted at very low q levels. Previous studies have

378   shown that as q approaches zero, vapor d-excess can approach 7000‰ following the Rayleigh distillation trajectory

379   (Bony et al., 2008), a behavior inherent to the definition of d-excess (Dütsch et al., 2017). High d-excess values

380   have also been observed in low humidity environments, ~~such as~~ polar regions (Bonne et al., 2014; Steen-Larsen et

381   al., 2017) and high altitudes (Samuels‐Crow et al., 2014; Webster and Heymsfield, 2003; Sayres et al., 2010;

382   Sodemann et al., 2017). Therefore, we infer that the increasing trend of d-excess with decreasing local q, upstream

383   q, and regional dew point temperature is due to enhanced mixing with dry and cold subsiding air transported by

384   westerlies from high altitudes. Relationships between upstream q and upstream air temperature as well as altitude

385   further support this inference, indicating that low humidity conditions are associated with the presence of subsiding

386   dry and cold air from high altitudes (Figs. 8c and 8d). Therefore, vapor d-excess during the non-monsoon not only

387   provides insights into specific humidity levels but also indicates the source of humidity.
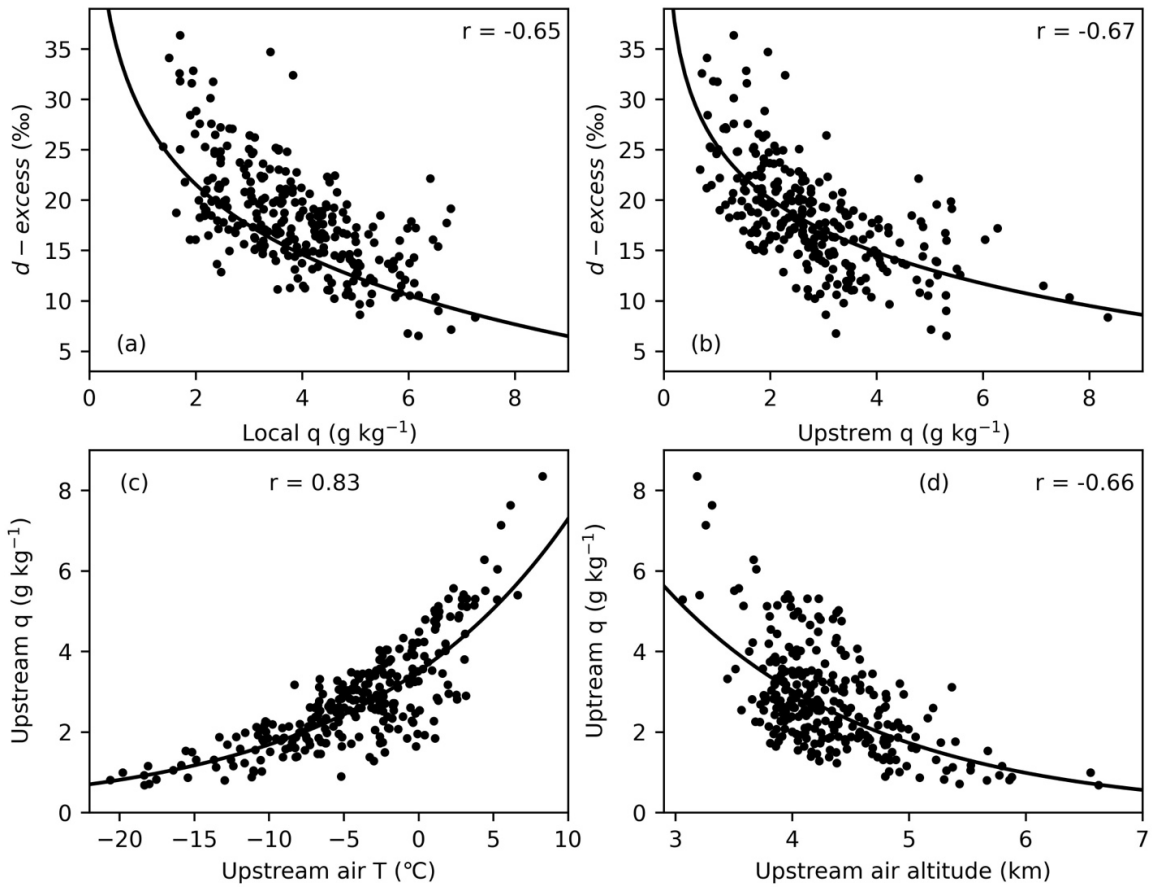
Figure 8. Relationships among vapor *d*-excess, local specific humidity (*q*), weighted-mean upstream *q*, weighted-mean upstream air temperature (T), and weighted-mean upstream air altitude during the non-monsoon season of November-April. (a) scatter plot of *d*-excess against local *q*. (b) scatter plot of *d*-excess against upstream weighted-mean *q*. (c) scatter plot of upstream *q* against upstream air T. (d) scatter plot of upstream *q* against upstream air altitude. All the upstream variables are mean values along backward trajectories weighted by the moisture contribution of air parcels. The solid curves indicate the log regression between the respective variables with the correlation coefficients indicated by the numbers.

396   **3.5 Role of rain-vapor interaction during the summer monsoon season**

397   In contrast to the significant dependence of *d*-excess on *q* during the non-monsoon season, ~~vapor *d*-excess~~

398   shows no correlation with q (r = 0.04, p = 0.51) during the summer monsoon season. The behavior of δ^{18}O also

399   differs between the two seasons (Fig. 3). During the summer monsoon season, δ^{18}O-q plots below the Rayleigh

400   curve, indicating that the vapor has ~~undergone a degree of rain-vapor interaction due to evaporation~~ (Fig. 3a). Partial

401   rain evaporation in an unsaturated atmospheric environment leads to kinetic fractionation, which decreases d-excess

402   values in raindrops while increasing d-excess in the surrounding vapor (Risi et al., 2008b). This effect of rain-vapor

403   interaction on vapor isotopes has been suggested as a primary mechanism driving the amount effect in tropical

404   regions (Risi et al., 2008a; Kurita et al., 2011; Bowen et al., 2019; Galewsky et al., 2016). Therefore, we hypothesize

405   that vapor isotopes during the summer monsoon season at SETP are influenced by the ~~degree~~ of rain-vapor

406   interaction.

407   The first evidence supporting this hypothesis is the significant correlation between δ^{18}O and d-excess during

408   the summer monsoon season (r = -0.55, p < 0.01; Fig. 9a). In ad~~dition, there is a trend where δ^{18}O and d-excess~~

409   ~~exhibit weaker correlations when δ^{18}O levels are high, and stronger correlations when δ^{18}O levels are low~~ (Figs. 9a

410   and S7). To explore this further, we categorized days with daily precipitation of at least 2 mm as "rainy days" and

411   those with less than 2 mm as "non-rainy days". This distinction is based on the premise that rain-vapor interaction

412   cannot occur in the absence of rainfall. The analysis reveals that δ^{18}O during rainy days is significantly lower than

413   that during non-rainy days, while d-excess show the opposite trend (p < 0.01 for both δ^{18}O and d-excess; Figs. 9b

414   and 9c). Furthermore, the correlation between δ^{18}O and d-excess becomes stronger on rainy days (r = -0.69, $p <$

415   0.01), though a weaker negative correlation persists even on non-rainy days (r = -0.40, $p < 0.01$). Even when

416   applying a stricter threshold of 0 mm for non-rainy days, the negative correlation between δ^{18}O and d-excess remains

417   significant (r = -0.37, p < 0.01). Moreover, correlations with local precipitation amount are weak for both δ^{18}O (r =

418   -0.31, p < 0.01) and d-excess (r = 0.26, p < 0.01). These findings lead us to infer that vapor isotopes during the

419   summer monsoon season at SETP are influenced not only by local rain-vapor interactions but also by the history of

420   rain-vapor interactions that occurred before the vapor reached the region.

421
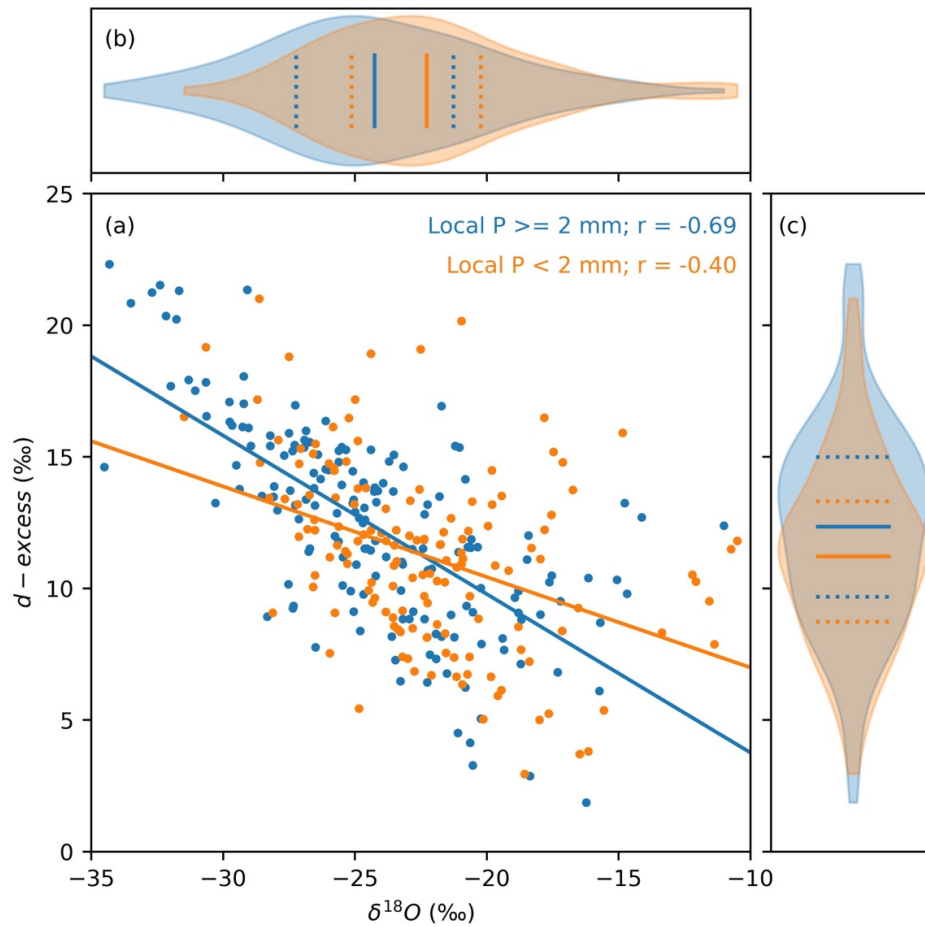
Figure 9. Relationships between SETP vapor *d*-excess and δ¹⁸O during the summer monsoon season. (a)

scatter plot of *d*-excess against δ¹⁸O and linear regression lines between them. (b) distribution of δ¹⁸O values

with the dashed lines indicate values at the lower and upper quartiles and the solid lines indicate the mean

values. (c) is the same as (b) but for *d*-excess. Orange colors indicate data observed during daily precipitation

amount less than 2 mm and blue colors indicate data observed during days with precipitation amount not

less than 2 mm. The r values for both lines are indicated in (a) and both of them are significant at the 0.01

level.

To further investigate the role of rain-vapor interactions, we use total precipitation amount (P_{acc}) as an indicator

of rain-vapor interaction, considering the cumulative effect over several days preceding sampling. Our analysis

431 examined correlations between vapor isotopes (δ^{18}O and d-excess) and P_{acc} for periods ranging from 1-10 days prior

432 to sampling (Figs. S8 and S9). Vapor d-excess reaches an optimal correlation with P_{acc} when considering 3 days

433 before sampling (P_{acc_3d}). Vapor δ^{18}O shows a slightly longer memory and reaches an optimal correlation around 5-

434 6 days before sampling. Fig. 10 shows the spatial distribution of these correlations, where d-excess positively

435 correlates with P_{acc_3d} across a ~5°×5° region surrounding SETP and extending southwestward to the Himalayas

436 (Fig. 10a). In contrast, δ^{18}O shows significant negative correlations in similar regions (Fig. 10b). Interestingly, even

437 on non-rainy days, significant regional-scale correlations persist, albeit weaker and with a smaller spatial extent

438 (Fig. S10).

439 These findings provide further evidence for understanding the mechanisms driving the amount effect. The

440 negative correlation between δ^{18}O and P_{acc} has also been observed in precipitation and can be attributed to either

441 continuous rainout (Scholl et al., 2009; Vuille et al., 2003; Ruan et al., 2019) or rain-vapor interactions (Lawrence

442 et al., 2004; Risi et al., 2008a; Kurita et al., 2011; Worden et al., 2007). While continuous rainout, explained by the

443 Rayleigh distillation model, accounts for the decreasing trend of δ^{18}O with increased rainfall, d-excess remains

444 relatively stable unless specific humidity drops to very low levels (~4 g kg^{-1} in Fig. 3b for example). The positive

445 correlation between vapor d-excess and P_{acc_3d} provides an additional constraint, suggesting that the amount effect

446 is not solely a result of rainout but also involves rain-vapor interactions, which significantly influence vapor isotopes

447 in the lower troposphere.

448
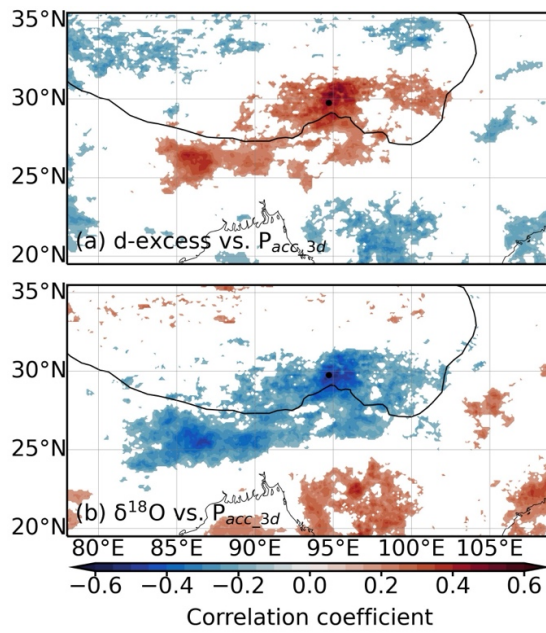
449 **Figure 10. Relationships between vapor isotops for rainy days (local daily precipitation amount not less**

450 **than 2 mm) and total precipitation amount at the regional scale during the summer monsoon season. (a)**

451 **spatial distribution of correlation coefficients between *d*-excess and total precipitation amount during 3 days**

452 **prior sampling (P_{acc_3d}). (b) is the same as (a) but for $\delta^{18}O$. Only values significant at the 95% significance**

453 **level are shown. The black dots indicate the location of the SETP station. The black solid lines denote the**

454 **Tibetan Plateau with altitude contour at 3000 m.**

455 **4 Implications for interpreting TP ice core isotope data**

456 Interpreting *d*-excess in meteoric water and ice cores on the TP is complicated by evaporation conditions over

457 the northern Indian Ocean (RH_{SST} and SST) and continental recycling (Shao et al., 2021; Zhao et al., 2012; Joswiak

458 et al., 2013; Pang et al., 2012; An et al., 2017). Attempts have been made to establish relationships between vapor

459 *d*-excess and RH_{STT} (Chen et al., 2024; Liu et al., 2024) as well as between ice core *d*-excess and RH_{STT} (Shao et al.,

460 2021) or SST (Zhao et al., 2012). Based on ~~results in Section 3.3,~~ however, the apparent relationships are primarily

461 a result of similarities in the seasonality of these variables.

462   Furthermore, the direct contribution of oceanic vapor to humidity at SETP is very limited (Fig. 4), implying an

463   even smaller contribution over the TP since SETP is at the forefront of moisture transport toward TP (Fig. S1). The

464   dominant terrestrial origin indicates significant continental recycling. Terrestrial processes such as transpiration and

465   evaporation introduce isotopically enriched moisture ~~and~~ high d-excess signatures, ~~respectively~~. Mixing with

466   terrestrial sources is also reflected in the relationship between vapor isotopes and q (Fig. 3). Seasonal changes and

467   long-term variations in precipitation and ice core isotopes have been interpreted as shifts in moisture source between

468   recycled terrestrial moisture and oceanic sources or their relative contributions (An et al., 2017; Yang and Yao, 2020).

469   Oceanic moisture is typically associated with the summer monsoon, while westerlies bring moisture from

470   continental recycling or even the Mediterranean Sea. Water isotope signatures on the TP were thought to reflect this

471   interplay between the summer monsoon and westerlies (Joswiak et al., 2013; Pang et al., 2012; Tian et al., 2007).

472   Despite seasonally shifting moisture sources, continental recycling prevails throughout the year (Fig. 4). Our

473   alternative perspective explains high d-excess induced by westerlies as dry and cold air intrusions rather than surface

474   evaporation or evapotranspiration. While the interplay between the summer monsoon and westerlies remains valid,

475   but we emphasize changes in air mass properties driven by different circulation systems.

476   The proposed alternative interpretation could also help explain the abnormally high d-excess in high-altitude

477   ice cores mentioned in the Introduction. This is because specific humidity at these ice core sites is extremely low,

478   and prolonged interaction with cold and dry air may further modify snow isotope compositions (Ma et al., 2024;

479   Wahl et al., 2022). In addition, intense rain-vapor interactions during the summer monsoon represent another

480   potential source of elevated d-excess (Section 3.5). When this high d-excess vapor contributes to subsequent

481   precipitation, its signal can be inherited in the resulting precipitation (Risi et al., 2008b). However, a clear

482   relationship between TP precipitation d-excess and monsoon convection has yet to be established, partly due to

483   limited attention paid to d-excess in previous studies. On the other hand, local raindrop evaporation may counteract

484 this effect by reducing raindrop d-excess values. The overall positive correlation between precipitation d-excess and

485 altitude across Asia has sometimes been attributed to stronger evaporation at lower altitudes (Bershaw, 2018). For

486 snowfall on glaciers, however, evaporation for falling snowflakes is less likely due to cold temperatures and the

487 short distance between the cloud base and the glacier surface. Therefore, elevated vapor d-excess signals caused by

488 accumulated rain-vapor interactions at upstream associated with monsoon convection could be a possible source of

489 the high d-excess in ice cores.

490 **5 Conclusions**

491 We present a three-year~~long~~ daily near-surface vapor isotope dataset ~~observed~~ at the SETP station, which is

492 at the major channel for moisture entering the TP. The paired measurements of vapor isotopes and specific humidity

493 reveal distinct moisture sources and dynamics between non-monsoon and summer monsoon seasons, consistent

494 with findings from Lagrangian moisture diagnostic. Despite significant negative correlations between d-excess and

495 relative humidity scaled to sea surface temperature over the northern Indian Ocean when all seasons are considered,

496 these correlations weaken or even disappear when analyzed within individual seasons. This finding challenges the

497 earlier interpretation of TP d-excess as indicator of oceanic evaporation conditions and guarantees new

498 interpretations in the future.

499 During the non-monsoon season, vapor d-excess is primarily influenced by specific humidity at both local and

500 upstream scales. Air that has undergone significant dehydration, situated at the lower end of the Rayleigh distillation,

501 is expected to have extremely high d-excess values. Backward trajectory analyses and moisture source diagnostics

502 reveal that the intrusion of cold and dry air driven by westerlies during the non-monsoon season leads to the

503 increasing trend in d-excess as specific humidity decreases. This process also contributes to a weak negative

504 correlation between d-excess and $\delta^{18}O$. Furthermore, $\delta^{18}O$ primarily reflects mixing processes involving a relatively

505 enriched moist end-member compared to the summer monsoon season. These new insights into vapor d-excess

506 during the non-monsoon season provide an alternative framework for interpreting the high d-excess in high-altitude

507 TP ice cores.

508 During the summer monsoon season, rain evaporation emerges as the dominant process shaping vapor isotope

509 compositions. First, $\delta^{18}O$ systematically shifts below the Rayleigh distillation curve, aligning with predictions of

510 "super-Rayleigh" distillation caused by partial rain evaporation. Second, $\delta^{18}O$ is anti-correlated with d-excess,

511 pointing to kinetic fractionation as a source of depleted vapor, which cannot be attributed solely to rainout. Third,

512 at the regional scale, $\delta^{18}O$ shows significant negative correlations with total precipitation amount, while d-excess

513 positively correlates with total precipitation amount. These findings enhance our understanding of atmospheric

514 humidity dynamics and help disentangle the different effects of rainout and rain-vapor interactions in the context of

515 the amount effect.

516 This study reveals distinct moisture sources and dynamics between non-monsoon and monsoon seasons over

517 the southeastern Tibetan Plateau. These findings will aid in interpreting $\delta^{18}O$ and d-excess records from Tibetan

518 Plateau glaciers, offering refined insights into past hydroclimatic conditions and challenging assumptions linking

519 ice core isotopes to oceanic evaporation alone.

520 **Competing interests**

521 The authors declare that they have no conflict of interest.

522 **Acknowledgements**

523 We thank the editors and the referees for their comments and suggesetions. This research was supported by the

524 National Key R&D Program of China (Grant 2024YFF0807901), the National Natural Science Foundation of China

525 (Grant 42371144), the Yunnan Fundamental Research Projects (Grant 202301AT070183), and the funding of

526   Donglu Talent Young Scholar from the Yunnan University and support for young scholars from the Double First-

527   Class Initiative for Ecological Disciplines of the Yunnan University. We would like to thank the staff at the South-

528   East Tibetan Plateau Station for integrated observation and research of alpine environment for their help in collecting

529   water samples and for sharing the meteorological data at the station.

530   **Data availability**

531   The NOAA ARL provided the HYSPLIT model and the GDAS data

532   (https://www.ready.noaa.gov/HYSPLIT.php). The Copernicus Climate Change Service provided the ERA5 data

533   (https://doi.org/10.24381/cds.adbb2d47 and https://doi.org/10.24381/cds.f17050d7). The GPM data are available

534   through GES DISC (https://doi.org/10.5067/GPM/IMERG/3B-HH/07). Local meteorological data at the SETP

535   station are provided by National Tibetan Plateau / Third Pole Environment Data Center

536   (https://dx.doi.org/10.11888/AtmosphericPhysics.tpe.68.db). The observation data at the SETP station have been

537   uploaded to Figshare and will be made publicly available after publication (10.6084/m9.figshare.27302871).

538   **Author contributions**

539   **Zhongyin Cai**: Conceptualization, methodology, investigation, formal analysis, funding acquisition, writing-

540   original draft, writing-review & editing; **Rong Li**: Investigation, data curation, writing-review & editing; **Cheng**

541   **Wang**: Validation; **Qiukai Mao**: Investigation, **Lide Tian**: Resources, project administration, funding acquisition.

542   **References**

543

544   Aemisegger, F., Pfahl, S., Sodemann, H., Lehner, I., Seneviratne, S. I., and Wernli, H.: Deuterium excess as a
545 proxy for continental moisture recycling and plant transpiration, Atmos. Chem. Phys., 14, 4029-4054, 10.5194/acp-
546 14-4029-2014, 2014.
547   An, W., Hou, S., Zhang, Q., Zhang, W., Wu, S., Xu, H., Pang, H., Wang, Y., and Liu, Y.: Enhanced Recent Local

548 Moisture Recycling on the Northwestern Tibetan Plateau Deduced From Ice Core Deuterium Excess Records, J.
549 Geophys. Res., 122, 12,541-512,556, 10.1002/2017jd027235, 2017.

550 Araguás-Araguás, L., Fröehlich, K., and Rozanski, K.: Stable isotope composition of precipitation over
551 southeast Asia, J. Geophys. Res., 103, 28721-28742, 1998.

552 Benetti, M., Reverdin, G., Pierre, C., Merlivat, L., Risi, C., Steen-Larsen, H. C., and Vimeux, F.: Deuterium excess
553 in marine water vapor: Dependency on relative humidity and surface wind speed during evaporation, J. Geophys.
554 Res., 119, 584-593, 2014.

555 Bershaw, J.: Controls on Deuterium Excess across Asia, Geosciences, 8, 257, 10.3390/geosciences8070257,
556 2018.

557 Bonne, J.-L., Behrens, M., Meyer, H., Kipfstuhl, S., Rabe, B., Schönicke, L., Steen-Larsen, H. C., and Werner, M.:
558 Resolving the controls of water vapour isotopes in the Atlantic sector, Nature Communications, 10, 1632,
559 10.1038/s41467-019-09242-6, 2019.

560 Bonne, J. L., Masson-Delmotte, V., Cattani, O., Delmotte, M., Risi, C., Sodemann, H., and Steen-Larsen, H. C.:
561 The isotopic composition of water vapour and precipitation in Ivittuut, southern Greenland, Atmos. Chem. Phys.,
562 14, 4419-4439, 10.5194/acp-14-4419-2014, 2014.

563 Bony, S., Risi, C., and Vimeux, F.: Influence of convective processes on the isotopic composition (δ^{18}O and δD)
564 of precipitation and water vapor in the tropics: 1. Radiative-convective equilibrium and Tropical Ocean–Global
565 Atmosphere–Coupled Ocean-Atmosphere Response Experiment (TOGA-COARE) simulations, J. Geophys. Res.,
566 113, D19305, 10.1029/2008JD009942, 2008.

567 Bowen, G. J. and Wilkinson, B.: Spatial distribution of δ^{18}O in meteoric precipitation, Geology, 30, 315,
568 10.1130/0091-7613(2002)030<0315:sdooim>2.0.co;2, 2002.

569 Bowen, G. J., Cai, Z., Fiorella, R. P., and Putman, A.: Isotopes in the Water Cycle: Regional- to Global-Scale
570 Patterns and Applications, Annu. Rev. Earth Planet. Sci., 47, 453-479, 10.1146/annurev-earth-053018-060220,
571 2019.

572 Breitenbach, S. F. M., Adkins, J. F., Meyer, H., Marwan, N., Kumar, K. K., and Haug, G. H.: Strong influence of
573 water vapor source dynamics on stable isotopes in precipitation observed in Southern Meghalaya, NE India, Earth
574 Planet. Sci. Lett., 292, 212-220, 10.1016/j.epsl.2010.01.038, 2010.

575 Cai, Z. and Tian, L.: Atmospheric controls on seasonal and interannual variations in the precipitation isotope
576 in the East Asian Monsoon region, J. Climate, 29, 1339-1352, 10.1175/JCLI-D-15-0363.1, 2016.

577 Cai, Z. and Tian, L.: What causes the post-monsoon ^{18}O depletion over Bay of Bengal head and beyond?,
578 Geophys. Res. Lett., 47, e2020GL086985, 10.1029/2020gl086985, 2020.

579 Cai, Z., Tian, L., and Bowen, G. J.: ENSO variability reflected in precipitation oxygen isotopes across the Asian
580 Summer Monsoon region, Earth Planet. Sci. Lett., 475, 25-33, 10.1016/j.epsl.2017.06.035, 2017.

581 Cai, Z., Tian, L., and Bowen, G. J.: Spatial-seasonal patterns reveal large-scale atmospheric controls on Asian
582 Monsoon precipitation water isotope ratios, Earth Planet. Sci. Lett., 503, 158-169, 10.1016/j.epsl.2018.09.028, 2018.

583 Cao, R., Huang, H., Wu, G., Han, D., Jiang, Z., Di, K., and Hu, Z.: Spatiotemporal variations in the ratio of
584 transpiration to evapotranspiration and its controlling factors across terrestrial biomes, Agr. Forest Meteorol., 321,
585 108984, 10.1016/j.agrformet.2022.108984, 2022.

586 Chen, M., Gao, J., Luo, L., Zhao, A., Niu, X., Yu, W., Liu, Y., and Chen, G.: Temporal variations of stable isotopic
587 compositions in atmospheric water vapor on the Southeastern Tibetan Plateau and their controlling factors, Atmos.
588 Res., 303, 10.1016/j.atmosres.2024.107328, 2024.

589 Craig, H.: Isotopic Variations in Meteoric Waters, Science, 133, 1702-1703, 10.1126/science.133.3465.1702,
590 1961.

591 Craig, H. and Gordon, L. I.: Deuterium and oxygen 18 variations in the ocean and the marine atmosphere, in:

592   Stable Isotopes in Oceanographic Studies and Paleotemperatures. Spoleto, Tongiorgi, E., Italy, 9-130, 1965.

593   Dai, D., Gao, J., Steen-Larsen, H. C., Yao, T., Ma, Y., Zhu, M., and Li, S.: Continuous monitoring of the isotopic
594 composition of surface water vapor at Lhasa, southern Tibetan Plateau, Atmos. Res., 264,
595 10.1016/j.atmosres.2021.105827, 2021.

596   Dansgaard, W.: Stable isotopes in precipitation, Tellus, 16, 436-468, 10.1111/j.2153-3490.1964.tb00181.x,
597 1964.

598   Dütsch, M., Pfahl, S., and Sodemann, H.: The impact of nonequilibrium and equilibrium fractionation on two
599 different deuterium excess definitions, J. Geophys. Res., 122, 12732-12746, 10.1002/2017JD027085, 2017.

600   Fiorella, R. P., Poulsen, C. J., and Matheny, A. M.: Seasonal Patterns of Water Cycling in a Deep, Continental
601 Mountain Valley Inferred from Stable Water Vapor Isotopes, J. Geophys. Res., 123, 7271-7291,
602 doi:10.1029/2017JD028093, 2018.

603   Galewsky, J., Steen-Larsen, H. C., Field, R. D., Worden, J., Risi, C., and Schneider, M.: Stable isotopes in
604 atmospheric water vapor and applications to the hydrologic cycle, Rev. Geophys., 54, 809-865,
605 10.1002/2015RG000512, 2016.

606   Good, S. P., Noone, D., and Bowen, G.: Hydrologic connectivity constrains partitioning of global terrestrial
607 water fluxes, Science, 349, 175-177, 10.1126/science.aaa5931, 2015.

608   Guo, H., Pang, H., Wu, S., Xu, T., Mutz, S. G., Zhan, Z., Lin, W., Zhang, W., and Hou, S.: Global abnormal
609 precipitation 18O depletion during late/post monsoon season, Earth Planet. Sci. Lett., 641,
610 10.1016/j.epsl.2024.118815, 2024.

611   Han, J., Tian, L., Cai, Z., Ren, W., Liu, W., Li, J., and Tai, J.: Season-specific evapotranspiration partitioning using
612 dual water isotopes in a Pinus yunnanensis ecosystem, southwest China, J. Hydrol., 608, 127672,
613 10.1016/j.jhydrol.2022.127672, 2022.

614   He, S., Jackisch, D., Feng, L., Samanta, D., Wang, X., and Goodkin, N. F.: Uncovering Below Cloud Rain-Vapor
615 Interactions During Tropical Rain Events Through Simultaneous and Continuous Real-Time Monitoring of Rain
616 and Vapor Isotopes, J. Geophys. Res., 129, e2023JD040084, https://doi.org/10.1029/2023JD040084, 2024.

617   He, Y., Risi, C., Gao, J., Masson-Delmotte, V., Yao, T., Lai, C.-T., Ding, Y., Worden, J., Frankenberg, C., Chepfer,
618 H., and Cesana, G.: Impact of atmospheric convection on south Tibet summer precipitation isotopologue
619 composition using a combination of in situ measurements, satellite data and atmospheric general circulation
620 modeling, J. Geophys. Res., 120, 3852-3871, 10.1002/2014JD022180, 2015.

621   Hersbach, H., Bell, B., Berrisford, P., Horányi, A., J., M.-S., Nicolas, J., Radu, R., Schepers, D., Simmons, A., Soci,
622 C., and Dee, D.: Global reanalysis: goodbye ERA-Interim, hello ERA5, 10.21957/vf291hehd7, 2019.

623   Huang, J.: A Simple Accurate Formula for Calculating Saturation Vapor Pressure of Water and Ice, Journal of
624 Applied Meteorology and Climatology, 57, 1265-1272, https://doi.org/10.1175/JAMC-D-17-0334.1, 2018.

625   Huffman, G. J., Stocker, E. F., Bolvin, D. T., Nelkin, E. J., and Tan, J.: GPM IMERG Final Precipitation L3 Half
626 Hourly 0.1 degree x 0.1 degree V07, Greenbelt, MD, Goddard Earth Sciences Data and Information Services Center
627 (GES DISC) [dataset], 10.5067/GPM/IMERG/3B-HH/07, 2023.

628   Immerzeel, W. W., Lutz, A. F., Andrade, M., Bahl, A., Biemans, H., Bolch, T., Hyde, S., Brumby, S., Davies, B. J.,
629 Elmore, A. C., Emmer, A., Feng, M., Fernández, A., Haritashya, U., Kargel, J. S., Koppes, M., Kraaijenbrink, P. D. A.,
630 Kulkarni, A. V., Mayewski, P. A., Nepal, S., Pacheco, P., Painter, T. H., Pellicciotti, F., Rajaram, H., Rupper, S., Sinisalo,
631 A., Shrestha, A. B., Viviroli, D., Wada, Y., Xiao, C., Yao, T., and Baillie, J. E. M.: Importance and vulnerability of the
632 world's water towers, Nature, 577, 364-369, 10.1038/s41586-019-1822-y, 2020.

633   Jiang, J., Zhou, T., Qian, Y., Li, C., Song, F., Li, H., Chen, X., Zhang, W., and Chen, Z.: Precipitation regime
634 changes in High Mountain Asia driven by cleaner air, Nature, 10.1038/s41586-023-06619-y, 2023.

635   Joswiak, D. R., Yao, T., Wu, G., Tian, L., and Xu, B.: Ice-core evidence of westerly and monsoon moisture

636   contributions in the central Tibetan Plateau, J. Glaciol., 59, 56-66, 10.3189/2013JoG12J035, 2013.

637   Keeling, C. D.: The concentration and isotopic abundances of atmospheric carbon dioxide in rural areas,
638   Geochim. Cosmochim. Acta, 13, 322-334, 10.1016/0016-7037(58)90033-4, 1958.

639   Kurita, N., Noone, D., Risi, C., Schmidt, G. A., Yamada, H., and Yoneyama, K.: Intraseasonal isotopic variation
640   associated with the Madden-Julian Oscillation, J. Geophys. Res., 116, D24101, 10.1029/2010JD015209, 2011.

641   Lawrence, J. R., Gedzelman, S. D., Dexheimer, D., Cho, H.-K., Carrie, G. D., Gasparini, R., Anderson, C. R.,
642   Bowman, K. P., and Biggerstaff, M. I.: Stable isotopic composition of water vapor in the tropics, J. Geophys. Res.,
643   109, D06115, 10.1029/2003JD004046, 2004.

644   Lee, J.-E. and Fung, I.: "Amount effect" of water isotopes and quantitative analysis of post-condensation
645   processes, Hydrol. Processes, 22, 1-8, 10.1002/hyp.6637, 2008.

646   Liu, F., Tian, L., Cai, Z., Wang, X., Liang, P., Wang, S., and Li, S.: What caused the lag between oxygen-18 and
647   deuterium excess in atmospheric vapor and precipitation during the earlier summer season in southwest China?,
648   J. Hydrol., 644, 10.1016/j.jhydrol.2024.132087, 2024.

649   Liu, J., Xiao, C., Ding, M., and Ren, J.: Variations in stable hydrogen and oxygen isotopes in atmospheric water
650   vapor in the marine boundary layer across a wide latitude range, Journal of Environmental Sciences, 26, 2266-
651   2276, 10.1016/j.jes.2014.09.007, 2014.

652   Luo, L.: Meteorological observation data from the integrated observation and research station of the alpine
653   environment in Southeast Tibet (2007-2017), National Tibetan Plateau Data Center [dataset],
654   10.11888/AtmosphericPhysics.tpe.68.db, 2018.

655   Ma, T., Jiang, Z., Ding, M., He, P., Li, Y., Zhang, W., and Geng, L.: A model framework for atmosphere–snow
656   water vapor exchange and the associated isotope effects at Dome Argus, Antarctica – Part 1: The diurnal changes,
657   The Cryosphere, 18, 4547-4565, 10.5194/tc-18-4547-2024, 2024.

658   Merlivat, L. and Jouzel, J.: Global climatic interpretation of the deuterium-oxygen 18 relationship for
659   precipitation, J. Geophys. Res., 84, 5029-5033, 1979.

660   Noone, D.: Pairing Measurements of the Water Vapor Isotope Ratio with Humidity to Deduce Atmospheric
661   Moistening and Dehydration in the Tropical Midtroposphere, J. Climate, 25, 4476-4494, 10.1175/jcli-d-11-
662   00582.1, 2012.

663   Pang, H., Hou, S., Kaspari, S., Mayewski, P., Introne, D., Masson-Delmotte, V., Jouzel, J., Li, Z., He, Y., Hong, S.,
664   and Qin, D.: Atmospheric circulation change in the central Himalayas indicated by a high-resolution ice core
665   deuterium excess record, Climate Research, 53, 1-12, 10.3354/cr01090, 2012.

666   Putman, A. L., Fiorella, R. P., Bowen, G. J., and Cai, Z.: A Global Perspective on Local Meteoric Water Lines:
667   Meta-analytic Insight into Fundamental Controls and Practical Constraints, Water Resour. Res., 55, 6896-6910,
668   10.1029/2019wr025181, 2019.

669   Risi, C., Bony, S., and Vimeux, F.: Influence of convective processes on the isotopic composition (δ^{18}O and δD)
670   of precipitation and water vapor in the tropics: 2. Physical interpretation of the amount effect, J. Geophys. Res.,
671   113, D19306, 10.1029/2008JD009943, 2008a.

672   Risi, C., Bony, S., Vimeux, F., Descroix, L., Ibrahim, B., Lebreton, E., Mamadou, I., and Sultan, B.: What controls
673   the isotopic composition of the African monsoon precipitation? Insights from event-based precipitation collected
674   during the 2006 AMMA field campaign, Geophys. Res. Lett., 35, L24808, 10.1029/2008GL035920, 2008b.

675   Ruan, J., Zhang, H., Cai, Z., Yang, X., and Yin, J.: Regional controls on daily to interannual variations of
676   precipitation isotope ratios in Southeast China: Implications for paleomonsoon reconstruction, Earth Planet. Sci.
677   Lett., 527, 115794, 10.1016/j.epsl.2019.115794, 2019.

678   Samuels-Crow, K. E., Galewsky, J., Sharp, Z. D., and Dennis, K. J.: Deuterium excess in subtropical free
679   troposphere water vapor: Continuous measurements from the Chajnantor Plateau, northern Chile, Geophys. Res.

680   Lett., 41, 8652-8659, 10.1002/2014gl062302, 2014.

681   Sayres, D. S., Pfister, L., Hanisco, T. F., Moyer, E. J., Smith, J. B., St. Clair, J. M., O'Brien, A. S., Witinski, M. F.,
682   Legg, M., and Anderson, J. G.: Influence of convection on the water isotopic composition of the tropical tropopause
683   layer and tropical stratosphere, J. Geophys. Res., 115, 10.1029/2009JD013100, 2010.

684   Scholl, M. A., Shanley, J. B., Zegarra, J. P., and Coplen, T. B.: The stable isotope amount effect: New insights
685   from NEXRAD echo tops, Luquillo Mountains, Puerto Rico, Water Resour. Res., 45, 10.1029/2008wr007515, 2009.

686   Shao, L., Tian, L., Cai, Z., Wang, C., and Li, Y.: Large-scale atmospheric circulation influences the ice core d-
687   excess record from the central Tibetan Plateau, Clim. Dyn., 57, 1805-1816, 10.1007/s00382-021-05779-9, 2021.

688   Sodemann, H., Schwierz, C., and Wernli, H.: Interannual variability of Greenland winter precipitation sources:
689   Lagrangian moisture diagnostic and North Atlantic Oscillation influence, J. Geophys. Res., 113,
690   10.1029/2007jd008503, 2008.

691   Sodemann, H., Aemisegger, F., Pfahl, S., Bitter, M., Corsmeier, U., Feuerle, T., Graf, P., Hankers, R., Hsiao, G.,
692   Schulz, H., Wieser, A., and Wernli, H.: The stable isotopic composition of water vapour above Corsica during the
693   HyMeX SOP1 campaign: insight into vertical mixing processes from lower-tropospheric survey flights, Atmos.
694   Chem. Phys., 17, 6125-6151, 10.5194/acp-17-6125-2017, 2017.

695   Steen-Larsen, H. C., Risi, C., Werner, M., Yoshimura, K., and Masson-Delmotte, V.: Evaluating the skills of
696   isotope-enabled General Circulation Models against in-situ atmospheric water vapor isotope observations, J.
697   Geophys. Res., 122, 246-263, 10.1002/2016JD025443, 2017.

698   Stein, A. F., Draxler, R. R., Rolph, G. D., Stunder, B. J. B., Cohen, M. D., and Ngan, F.: NOAA's HYSPLIT
699   atmospheric transport and dispersion modeling system, Bull. Am. Meteorol. Soc., 96, 2059-2077, 10.1175/BAMS-
700   D-14-00110.1, 2015.

701   Terzer-Wassmuth, S., Wassenaar, L. I., Welker, J. M., and Araguas-Araguas, L. J.: Improved High-Resolution
702   Global and Regionalized Isoscapes of δ18O, δ2H, and d-Excess in Precipitation, Hydrol. Processes, 35,
703   10.1002/hyp.14254, 2021.

704   Thompson, L. G., Yao, T., E.Mosley-Thompson, Davis, M. E., Henderson, K. A., and Lin, P.-N.: A High-
705   Resolution Millennial Record of the South Asian Monsoon from Himalayan Ice Cores, Science, 289, 1916-1919,
706   10.1126/science.289.5486.1916, 2000.

707   Thompson, L. G., Yao, T. D., Davis, M. E., Mosley-Thompson, E., Synal, H. A., Wu, G., Bolzan, J. F., Kutuzov, S.,
708   Beaudon, E., Sierra-Hernández, M. R., and Beer, J.: Ice core evidence for an orbital-scale climate transition on the
709   Northwest Tibetan Plateau, Quat. Sci. Rev., 324, 10.1016/j.quascirev.2023.108443, 2024.

710   Tian, L., Masson-Delmotte, V., Stievenard, M., Yao, T., and Jouzel, J.: Tibetan Plateau summer monsoon
711   northward extent revealed by measurements of water stable isotopes, J. Geophys. Res., 106, 28081-28088,
712   10.1029/2001JD900186, 2001.

713   Tian, L., Yao, T., MacClune, K., White, J. W. C., Schilla, A., Vaughn, B., Vachon, R., and Ichiyanagi, K.: Stable
714   isotopic variations in west China: A consideration of moisture sources, J. Geophys. Res., 112, D10112,
715   10.1029/2006jd007718, 2007.

716   Tian, L., Yu, W., Schuster, P. F., Wen, R., Cai, Z., Wang, D., Shao, L., Cui, J., and Guo, X.: Control of seasonal
717   water vapor isotope variations at Lhasa, southern Tibetan Plateau, J. Hydrol., 580, 124237,
718   10.1016/j.jhydrol.2019.124237, 2020.

719   Uemura, R., Matsui, Y., Yoshimura, K., Motoyama, H., and Yoshida, N.: Evidence of deuterium excess in water
720   vapor as an indicator of ocean surface conditions, J. Geophys. Res., 113, 10.1029/2008jd010209, 2008.

721   Vuille, M., Bradley, R. S., Werner, M., Healy, R., and Keimig, F.: Modeling δ^{18}O in precipitation over the tropical
722   Americas: 1. Interannual variability and climatic controls, J. Geophys. Res., 108, 4174, 10.1029/2001JD002038, 2003.

723   Wahl, S., Steen-Larsen, H. C., Hughes, A. G., Dietrich, L. J., Zuhr, A., Behrens, M., Faber, A.-K., and Hörhold,

M.: Atmosphere-Snow Exchange Explains Surface Snow Isotope Variability, Geophys. Res. Lett., 49, e2022GL099529, 10.1029/2022GL099529, 2022.

Webster, C. R. and Heymsfield, A. J.: Water isotope ratios D/H, 18O/16O, 17O/16O in and out of clouds map dehydration pathways, Science, 302, 1742-1745, 10.1126/science.1089496, 2003.

Wei, Z. and Lee, X.: The utility of near-surface water vapor deuterium excess as an indicator of atmospheric moisture source, J. Hydrol., 123923, 10.1016/j.jhydrol.2019.123923, 2019.

Welp, L. R., Lee, X., Griffis, T. J., Wen, X. F., Xiao, W., Li, S., Sun, X., Hu, Z., Val Martin, M., and Huang, J.: A meta-analysis of water vapor deuterium-excess in the midlatitude atmospheric surface layer, Global Biogeochem. Cycles, 26, 10.1029/2011gb004246, 2012.

Worden, J., Noone, D., and Bowman, K.: Importance of rain evaporation and continental convection in the tropical water cycle, Nature, 445, 528-532, 10.1038/nature05508, 2007.

Yang, X. and Yao, T.: Seasonality of moisture supplies to precipitation over the Third Pole: a stable water isotopic perspective, Sci Rep, 10, 15020, 10.1038/s41598-020-71949-0, 2020.

Yang, X., Davis, M. E., Acharya, S., and Yao, T.: Asian monsoon variations revealed from stable isotopes in precipitation, Clim. Dyn., 51, 2267-2283, 10.1007/s00382-017-4011-4, 2017.

Yao, T., Masson-Delmotte, V., Gao, J., Yu, W., Yang, X., Risi, C., Sturm, C., Werner, M., Zhao, H., He, Y., Ren, W., Tian, L., Shi, C., and Hou, S.: A review of climatic controls on δ^{18}O in precipitation over the Tibetan Plateau: Observations and simulations, Rev. Geophys., 51, 525-548, 10.1002/rog.20023, 2013.

Yao, T., Bolch, T., Chen, D., Gao, J., Immerzeel, W., Piao, S., Su, F., Thompson, L., Wada, Y., Wang, L., Wang, T., Wu, G., Xu, B., Yang, W., Zhang, G., and Zhao, P.: The imbalance of the Asian water tower, Nature Reviews Earth & Environment, 3, 618-632, 10.1038/s43017-022-00299-4, 2022.

Yu, W., Tian, L., Ma, Y., Xu, B., and Qu, D.: Simultaneous monitoring of stable oxygen isotope composition in water vapour and precipitation over the central Tibetan Plateau, Atmos. Chem. Phys., 15, 10251-10262, 10.5194/acp-15-10251-2015, 2015.

Yu, W., Tian, L., Risi, C., Yao, T., Ma, Y., Zhao, H., Zhu, H., He, Y., Xu, B., Zhang, H., and Qu, D.: δ^{18}O records in water vapor and an ice core from the eastern Pamir Plateau: Implications for paleoclimate reconstructions, Earth Planet. Sci. Lett., 456, 146-156, 10.1016/j.epsl.2016.10.001, 2016.

Zhang, Q., Shen, Z., Pokhrel, Y., Farinotti, D., Singh, V. P., Xu, C.-Y., Wu, W., and Wang, G.: Oceanic climate changes threaten the sustainability of Asia's water tower, Nature, 615, 87-93, 10.1038/s41586-022-05643-8, 2023.

Zhang, Q., Shen, Z., Pokhrel, Y., Farinotti, D., Singh, V. P., Xu, C.-Y., Wu, W., and Wang, G.: Reply to: Atlantic oceanic droughts do not threaten Asian water tower, Nature, 638, E16-E18, 10.1038/s41586-024-08358-0, 2025.

Zhao, H., Xu, B., Li, Z., Wang, M., Li, J., and Zhang, X.: Abundant climatic information in water stable isotope record from a maritime glacier on southeastern Tibetan Plateau, Clim. Dyn., 48, 1161-1171, 10.1007/s00382-016-3133-4, 2017.

Zhao, H., Xu, B., Yao, T., Wu, G., Lin, S., Gao, J., and Wang, M.: Deuterium excess record in a southern Tibetan ice core and its potential climatic implications, Clim. Dyn., 38, 1791-1803, 10.1007/s00382-011-1161-7, 2012.

Zhao, Y., Xu, C., Yu, X., Liu, Y., and Ji, X.: Atlantic oceanic droughts do not threaten Asian water tower, Nature, 638, E13-E15, 10.1038/s41586-024-08357-1, 2025.